Efficient Heart Sound Segmentation and Extraction Using Ensemble Empirical Mode Decomposition and Kurtosis Features

Chrysa D. Papadaniil, *Student Member, IEEE*, and Leontios J. Hadjileontiadis, *Senior Member, IEEE*

***Abstract*—An efficient heart sound segmentation (HSS) method that automatically detects the location of first (S_1) and second (S_2) heart sound and extracts them from heart auscultatory raw data is presented here. The heart phonocardiogram is analyzed by employing ensemble empirical mode decomposition (EEMD) combined with kurtosis features to locate the presence of S_1, S_2, and extract them from the recorded data, forming the proposed HSS scheme, namely HSS-EEMD/K. Its performance is evaluated on an experimental dataset of 43 heart sound recordings performed in a real clinical environment, drawn from 11 normal subjects, 16 patients with aortic stenosis, and 16 ones with mitral regurgitation of different degrees of severity, producing 2608 S_1 and S_2 sequences without and with murmurs, respectively. Experimental results have shown that, overall, the HSS-EEMD/K approach determines the heart sound locations in a percentage of 94.56% and segments heart cycles correctly for the 83.05% of the cases. Moreover, results from a noise stress test with additive Gaussian noise and respiratory noises justify the noise robustness of the HSS-EEMD/K. When compared with four other efficient methods that mainly employ wavelet transform, energy, simplicity, and frequency measures, respectively, using the same experimental database, the HSS-EEMD/K scheme exhibits increased accuracy and prediction power over all others at the level of 7–19% and 4–9%, respectively, both in controls and pathological cases. The promising performance of the HSS-EEMD/K paves the way for further exploitation of the diagnostic value of heart sounds in everyday clinical practice.**

***Index Terms*—Ensemble empirical mode decomposition (EEMD), first and second heart sound, heart sound segmentation (HSS), HOS, kurtosis, phonocardiogram (PCG).**

I. Introduction

HEART auscultation, i.e., the act of listening with a stethoscope to sounds produced by the heart, lungs, and blood, is an essential part of the physical examination and can provide information about the rate and rhythm, valve functioning, and anatomical defects of the heart. It has been used as an official diagnostic method since Laennec invented the first stethoscope in 1816 [1]. The most recent development in auscultation is the use of electronic stethoscopes that convert the acoustic sound waves to electrical signals, which can then be amplified and processed for optimal listening. However, heart auscultation and interpretation of its findings still depend on the subjectivity and the training of the human ear, due to the lack of a fully automated diagnosis tool; hence, doctors have to perform this task on their own. The preponderant methods of inspecting the heart condition are the ECG and the ultrasound; they are, though, compared to auscultation, less cost-effective and with more hardware demands. Thus, auscultation constitutes the most suitable heart examination method for primary health care, where simplicity and low cost are particularly appreciated.

The heart functions by repeating cycles of systole and diastole. During systole, the heart chambers eject blood, while during diastole, the heart chambers are filled with blood. This periodicity is also found in the heart sounds, where a first sound, i.e., S_1, is heard at the beginning of systole, while a second sound, i.e., S_2, is heard at the beginning of diastole. Generally, the mechanisms responsible for the heart sound productions cause eddies in the vascular system and produce vibrations that are audible. S_1 and S_2 constitute the normal heart sounds and both result from the closing of the valves at each heart period (mitral and tricuspid valves before systole, aortic and pulmonic valves before diastole). Nevertheless, there are other sounds that might be heard as a result of irregular blood flow and may have a pathological cause or not. These are S_3, S_4, and a category of sounds, called murmurs, that is associated with valve dysfunctions. There are many kinds of murmurs, defined by the following characteristics: location where the murmur is best heard, loudness (depending on the height of the sound wave), frequency (depending on the wave cycles generated per second), quality of sound, timing (systolic or diastolic), and possible radiation to other chest areas. Two of the most frequently met dysfunctions that cause murmurs are the aortic stenosis and the mitral regurgitation [2].

The acoustic signal produced by the heart sounds can be visually depicted in the phonocardiogram (PCG). Representative cases of heart sound signals are depicted in Fig. 1. Digital signal processing techniques can then be applied to the PCG as a means for analysis, information extraction, and processing. A first step in the analysis of the PCG is the heart sound segmentation (HSS), which is the division of the heart cycle into its four components, i.e., diastole-S_1-systole-S_2, or, equivalently, the identification of the positions of S_1 and S_2. Using the ECG as an auxiliary signal to perform this task may serve as a reference

Manuscript received February 1, 2013; revised October 10, 2013; accepted November 30, 2013. Date of publication December 11, 2013; date of current version June 30, 2014.

C. D. Papadaniil is with the Department of Electrical and Computer Engineering, Aristotle University of Thessaloniki, GR 54006 Thessaloniki, Greece (e-mail: chrysa.papadaniil@gmail.com).

L. J. Hadjileontiadis is with the Department of Electrical and Computer Engineering, Aristotle University of Thessaloniki, GR-54006 Thessaloniki, Greece, and also with the State Conservatory of Thessaloniki, GR-54625 Thessaloniki, Greece (e-mail: leontios@auth.gr).

Digital Object Identifier 10.1109/JBHI.2013.2294399

2168-2194 © 2013 IEEE. Personal use is permitted, but republication/redistribution requires IEEE permission.
See http://www.ieee.org/publications_standards/publications/rights/index.html for more information.

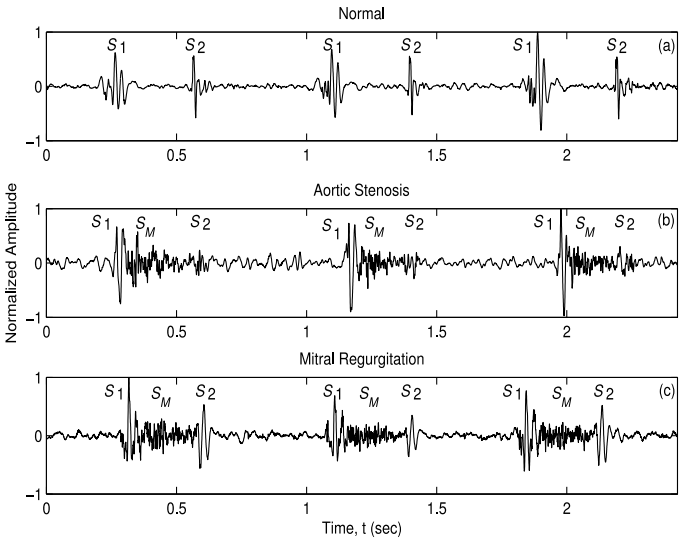

Fig. 1. PCG of three heart sound sequences from: (a) controls, (b) a case of medium aortic stenosis, and (c) a case of severe mitral regurgitation. S_1 and S_2 represent the first and the second heart sound, respectively, while S_M denotes the systolic murmur in (b) aortic stenosis and in (c) mitral regurgitation.

for the detection of the sounds; however, this study is mainly interested in the purely phonocardiographic approaches.

Up to now, a number of HSS schemes have been reported in the literature. Many of them are based on wavelet transform (WT) analysis, that, using a basis function, progressively decomposes a signal into its low- and high-frequency characteristics, namely the approximation and detail coefficients, respectively [3]–[8]. In particular, Chebil and Al-Nabulsi suggested the Discrete WT (DWT) decomposition/reconstruction of the PCG signal to form an HSS-DWT scheme, where the peak values of S_1 are identified using the approximation coefficients, while the peak values of S_2 emerge from the reconstructed detail approximations [3]. Matching pursuit, a decomposition analysis based on the WT, has been considerably used for the time–frequency analysis of the PCG, for distinguishing murmurs from normal heart sounds, for determining the degree of normality of a sound, and for the independent segmentations of S_1 and S_2 into their components [9]–[13]. Another widely applied method involves calculating the Shannon energy of the recorded PCG signal [14], [15]. In particular, Ari *et al.* took into account the energy content of the heart sounds and their time topology and suggested a robust and simple HSS algorithm (HSS-ET) [15]. In study [8], both WT and energy of the PCG were employed to detect different heart sounds, while in [16], the events of the cardiac cycle were detected through the envelopes of amplitude, energy, and frequency of the PCG. Naseri *et al.* distinguished the PCG components based on an expert frequency–energy-based metric, forming the HSS-FEM scheme [17]. These approaches lie in the general case of calculating the envelope of the PCG to detect its peaks. A comparison study of the envelope extraction methods was performed in [18], including the Shannon energy, the Hilbert–Huang transform (HHT), and the characteristic waveform of the PCG. Analysis of the heart sounds based on the HHT has been presented in [19] and [20], while a detection method of the third and the fourth heart sounds based on the HHT was presented in [21]. Another envelope-based method for pediatric HSS was described in [22], where the envelope is obtained through short-time spectral energy and autoregressive parameters of the signal and the detected sounds are classified using a Multilayer Perceptron classifier. Furthermore, in [23], the Viola integral method was used to calculate the characteristic and the characteristic moment waveforms, while the sounds' cyclical characteristics were considered for the HSS. Nigam and Priemer have presented a simplicity-based method for PCG segmentation, which uses inherent complexity of the heart sound components [24]. Then, Vepa *et al.* proposed an HSS-ETS scheme using energy, simplicity, and timing information, yielding better results with an accuracy up to 84% [25]. A different approach was suggested in [26], where homomorphic filtering and k-Means were used for HSS. Gamero and Watrous, as well as Gill *et al.*, have proposed a probabilistic approach for detecting S_1 and S_2, by employing Hidden Markov Models (HMMs) to model the systole and diastole periods [27], [28]. Duration-dependent HMMs were recently introduced to improve the segmentation performance of the HMMs [29], but were not tested on patients with valve disease. Fuzzy logic was also used in an arrhythmias detection-oriented HSS method [30]. Finally, Tang *et al.* introduced dynamic clustering based on density function after decomposing the PCG signal into atoms [31].

The majority of the aforementioned methods focuses on the energy and frequency properties of the signal. However, detection through these techniques requires selection of thresholds and parameters, which are commonly not much motivated or excessively depending on the available datasets characteristics. Another commonplace impropriety is that heart sounds features reported in the literature, concerning the S_1 and S_2 frequency range, or the S_1 and S_2 durations, are applied too tightly, resulting in misinterpreting the sounds that are deviating from the expected ranges, especially in valve diseases cases, where sounds features are frequently altered. It is therefore preferable to decompose the signal into its own fluctuations rather than filter it based on fixed values. This is most probably the motivation behind the WT HSS schemes; however, wavelets employ predetermined decomposition scales. An alternative, adaptive, and data-driven decomposition is the intention of this study, as it is expected to adjust more to the waveforms characteristics.

This study proposes a novel HSS method that uses ensemble empirical mode decomposition (EEMD) [32] to analyze heart sounds into intrinsic mode functions (IMFs) along with kurtosis statistics, to detect the abrupt changes, that the occurrences of S_1 and S_2 cause to the derived IMFs. EEMD is a noise-assisted data analysis that evolved from empirical mode decomposition (EMD) [33]. According to Wu and Huang, the EEMD enables the EMD to be a true dyadic filter for any data [32]. The merits of analyzing the heart sounds by IMFs have been presented in [20] and [34], while Boutana *et al.* proposed optimal IMFs for the denoising of the heart sound signals [35]. EMD has been suggested as a feature extraction method in [36], and has been used as such in [37], to classify the segmented sounds drawn from [15] into different pathologies. Recently, EEMD-based

feature extraction was adopted in a system that utilizes recorded heart sounds and electrocardiogram signals to automatically distinguish between normal and abnormal heart conditions [38]. The aim of this study is to use EEMD to segment the cardiac cycle before proceeding to the sounds classification, so that the two steps do not employ more than one signal analysis method. The increased quality of the segmented and extracted S_1 and S_2 provides the physician with an enhanced source of diagnostic information, available at the everyday clinical practice, and adds to the realization of a full-cycle process, i.e., data acquisition, data segmentation/de-noising, feature extraction, and classification. In addition, kurtosis has often been used in the signal processing field due to its ability to detect the changes of a waveform [39], [40]. The proposed HSS method, namely HSS-EEMD/K has been applied on a database that includes heart sounds from normal subjects and sounds from patients with aortic stenosis and mitral regurgitation, with embedded murmurs that make the S_1 and S_2 discrimination and extraction from the PCG data harder. The experimental results have shown a promising performance, elaborated further by a noise stress test and the comparison analysis among the performance of HSS-DWT [3], HSS-ET [15], HSS-FEM [17], HSS-ETS [25], and HSS-EEMD/K, from which the proposed approach exhibits increased accuracy and prediction power versus all other four ones.

The rest of this paper is structured as follows. Section II introduces a mathematical background, whereas Section III describes the proposed approach. Section IV discusses some experimental and implementation issues, while Section V presents and discusses the experimental, noise stress test, and comparison analysis results obtained. Finally, Section VI concludes the paper.

II. Mathematical Background

A. Empirical Mode Decomposition

Contrary to previous methods, EMD does not use an *a priori* basis of expansion, as it is entirely data driven. The main idea behind it is that all data consist of different simple intrinsic modes of oscillations, represented by the IMFs. An IMF has to satisfy two conditions: 1) in the whole raw data, the numbers of extrema and zero-crossings must either be equal or differ at most by one, and 2) at any point, the mean value of the envelope defined by the local maxima and the envelope defined by the local minima is zero [33]. The EMD method analyzes the signal at its local oscillation scale, subtracts the faster oscillation, and iterates on the residual. The algorithm for producing the L-empirical modes (IMFs) from a given signal $x(t)$ is called a sifting process [33] and allows for the signal to be expressed as:

$$x(t) = \sum_{\lambda=1}^{L} IMF_{\lambda}(t) + r_L(t) \tag{1}$$

where $IMF_{\lambda}(t)$ denotes the λth IMF and $r_L(t)$ is a final (trend-like) residue.

B. Ensemble EMD

EEMD has been proposed to remedy the problem of mode mixing, occurring in EMD [32]. In a mode mixing case, different modes of oscillation may appear in one IMF or one mode can spread across different IMFs, depriving the IMFs of physical meaning. In EEMD, an ensemble mean is taken from a number of IMFs extracted from multiple applications of EMD to the original data, with the addition of white noise series. The added noise occupies the entire time–frequency space and the parts of the signal are automatically projected onto proper scales of reference established by the white noise, thus, eliminating the mode mixing effect. The ensemble mean of a number of corresponding IMFs will leave only the IMF signal, as a collection of white noise cancels each other out in a time-space ensemble mean [32].

C. Kurtosis

The kurtosis of a fourth-order stationary, zero-mean, stochastic process $x(t)$ is defined as the fourth-order cumulant for zero-lag [41]. The kurtosis parameter is merely estimated using a finite-length time-window and its value depends on the length of the sample. Thus, the kurtosis estimate is authorized to exist in a confidence interval, which is conditioned by the probability properties of the estimator. Asymptotically, this could give the exact value of the kurtosis; both real-life applications and transients are, however, temporally bounded. Hence, one has to determine both a lower and an upper bound for the estimator. Given a desired confidence interval, the estimator can be framed between two values, depending on the first statistics of the estimator. For the X random variable ($X \in x(t)$) of mean μ and standard deviation σ, the Chebyshev inequality [42] yields a lower bound of the probability that exists inside an interval centered at μ and having a diameter 2ε, i.e.,

$$P\Big\{X \in \Big(\mu - \frac{\sigma}{\sqrt{1-q}}, \mu + \frac{\sigma}{\sqrt{1-q}}\Big)\Big\} > q \tag{2}$$

where $q = 1 - (\sigma^2/\epsilon^2)$, $\epsilon > 0$, and σ^2/ϵ^2 is sufficiently small. Let $x(n)$ be a zero-mean, N-sample observation from a random variable X. The kurtosis estimate $\hat{\gamma}_4$ of $x(n)$ is given by [41]

$$\hat{\gamma}_4 = (N-1)\frac{\sum_{n=1}^{N} x^4(n)}{\big(\sum_{n=1}^{N} x^2(n)\big)^2}. \tag{3}$$

Additionally, if X is assumed to be Gaussian, then it is easy to show that [43]

$$\hat{m} \approx \frac{6}{N} \text{ and } \hat{s}^2 \approx \frac{24}{N} \tag{4}$$

where $\hat{m}$ and $\hat{s}$ are the mean and the standard deviation estimates of $\hat{\gamma}_4$, respectively. Substitutions of the expressions (4) into (2) yields in

$$P\big\{\hat{\gamma}_4 \in I(N,q)\big\} > q \tag{5}$$

where

$$I(N,q) = \left(\frac{6}{N} - \sqrt{\frac{24}{N(1-q)}}, \frac{6}{N} + \sqrt{\frac{24}{N(1-q)}}\right) \tag{6}$$

concluding that if the kurtosis estimate of a N-sample observation $x(n)$ lies outside $I(N,q)$, then it is natural to assume that $x(n)$ does not follow a Gaussian distribution. It could be hypothesized that in the absence of heart sounds, the PCG signal follows a Gaussian or at least symmetrical distribution, while when a heart sound occurs it does not. This concept is transferred to the EEMD domain, twofolds: 1) as a means to select [using (6)] the IMFs that embed the frequency content of the heart sounds (frequency-domain characteristic-selection across IMFs) and 2) as a means to extract the segments of the selected IMFs that deviate from Gaussianity, thus detecting the time-locked heart sound occurrences (time-domain characteristic-selection within IMFs). With a simple reconstruction of the selected IMFs and the corresponding segments, the extraction of the heart sound from the background PCG signal is feasible. These ideas are the core rationale behind the proposed HSS-EEMD/K approach.

III. Proposed HSS-EEMD/K Scheme

A. Preprocessing

A schematic representation of the complete proposed HSS-EEMD/K scheme is presented in Fig. 2, combined with a working example (see Fig. 3). Median and low-pass filtering is initially applied to the normalized, zero-mean N-sample PCG signal, denoted by $x[n]$ ($n = 1, \ldots, N$). A third-order median filter is used to enhance the quality of the acquired signal, followed by a tenth-order low-pass Butterworth filter with a cutoff frequency of 150 Hz, producing the filtered signal $x_f[n]$ ($n = 1, \ldots, N$). Reduction of the high-frequency noise and the high-frequency murmur effect facilitates the detection of S_1 and S_2, whose major energy concentrations lie below 150 Hz [44].

B. EEMD-Based IMFs Estimation and Selection

The filtered PCG signal $x_f[n]$ ($n = 1, \ldots, N$) is then decomposed into L IMF components using EEMD. The IMFs are denoted by $IMF_\lambda[n]$ ($\lambda = 1, \ldots, L$), while the residual is denoted by $r_L[n]$ ($n = 1, \ldots, N$). Since each sequential IMF contains lower frequency oscillations than the one extracted before, the frequency heart sound components are distributed across different IMFs. Fig. 3(i) presents an example of an original PCG signal $x[n]$ [see Fig. 3(i)–(a)], the filtered signal $x_f[n]$ [see Fig. 3(i)–(b)], and the first six IMFs extracted by the EEMD application on the latter [see Fig. 3(i)–(c):(h)]. Then, a three-criteria test is performed to select the IMFs that contain the S_1 and S_2 important components, so that further analysis is performed only on them.

1) Energy-Based Criterion: This criterion aims to exclude the IMFs that do not enclose significant energy concentration related to S_1 and S_2. The ratio

$$\eta_\lambda = \frac{E\left\{\left(\sum_{\lambda=1}^{M_\eta} IMF_\lambda[n]\right)^2\right\}}{E\left\{(x_f[n])^2\right\}} \tag{7}$$

where $1 \leq M_\eta \leq L, n = 1, \ldots, N$ and $E\{\cdot\}$ denotes the mean value operator, evaluates the energy contribution of each IMF normalized to the total energy of the $x_f[n]$. The η_λ parameter is iteratively calculated until it exceeds a threshold value, determining the first M_η IMFs that contain the largest part of the filtered signals energy. Thus, an Ω_η set of the selected M_η IMFs is formed as

$$\Omega_\eta = \{IMF\eta[n]\} \tag{8}$$

where $\eta = 1, \ldots, M_\eta$.

2) Instantaneous Frequency-Based Criterion: The second criterion eliminates the IMFs whose mean instantaneous frequency, denoted by *MIF* does not correspond to the S_1, S_2 frequency content. As mentioned earlier, the major concentrations of energy of both S_1 and S_2 lie below 150 Hz. To this end, the *MIF* of each IMF is calculated and a threshold is applied to select the last M_F IMFs with an *MIF* of less than 150 Hz ($1 \leq M_F \leq L$). The second selected set of IMFs is denoted by

$$\Omega_F = \{IMF_F[n]\} \tag{9}$$

where $F = L - M_F + 1, \ldots, L$. In this way, the additive high-frequency noise and the high-frequency components of present murmurs that were not removed by the preprocessing filtering are eliminated.

3) Bootstrap Kurtosis-Based Criterion: The third criterion employs the Gaussianity test that was previously analyzed (see Section II-C). Given a specific probability q, the confidence interval $I(N,q)$ is calculated using (6). Then, using (3) and the Bootstrap method [45] for b times, the kurtosis estimate of each N-sample IMF is computed as

$$\hat{\gamma}_4^{\lambda,b} = (N-1)\frac{\sum_{n=1}^{N} IMF_\lambda^4[n]}{\left(\sum_{n=1}^{N} IMF_\lambda^2[n]\right)^2} \tag{10}$$

where $\lambda = 1, \ldots, L$. The mean $\hat{\gamma}_4^{\lambda,b}$ for each IMF, denoted by $E\{\hat{\gamma}_4^{\lambda,b}\}$, is extracted and compared to $I(N,q)$. If $E\{\hat{\gamma}_4^{\lambda,b}\}$ lies outside the confidence interval, then the λth IMF does not follow the Gaussian distribution and, thus, it is expected to contain the heart sound occurrence content. The M_K ($1 \leq M_K \leq L$) IMFs that satisfy the third criterion comprise the Ω_K set, so that

$$\Omega_K = \{IMF_K[n]\} \tag{11}$$

where $1 \leq K \leq L$. The final selected set of M IMFs, denoted by $sIMF$ is the one that fulfills all three criteria; hence,

$$sIMF_m[n] = \Omega_\eta \cap \Omega_F \cap \Omega_K \tag{12}$$

where $m = 1, \ldots, M$, $1 \leq M \leq \min(M_\eta, M_F, M_K)$, and $n = 1, \ldots, N$. The selection procedure for the IMFs of Fig. 3(i) is shown in Fig. 3(ii).

C. Kurtosis-Based S_1 and S_2 Detection

The primary heart sounds of the PCG signal are located using an algorithm based on the calculation of the kurtosis estimate across the selected IMFs. This algorithm consists of the following steps:

1) Kurtosis Estimate Calculation: W sliding windows of lengths l_w ($w = 1, \ldots, W$) are applied on the N-sample $sIMF$ set and the kurtosis estimate is calculated using (4), as

$$\hat{\gamma}_4^{m,l_w}[k] = (l_w - 1)\frac{\sum_{n=1}^{l_w} sIMF_m^4[n]}{\left(\sum_{n=1}^{l_w} sIMF_m^2[n]\right)^2} \tag{13}$$

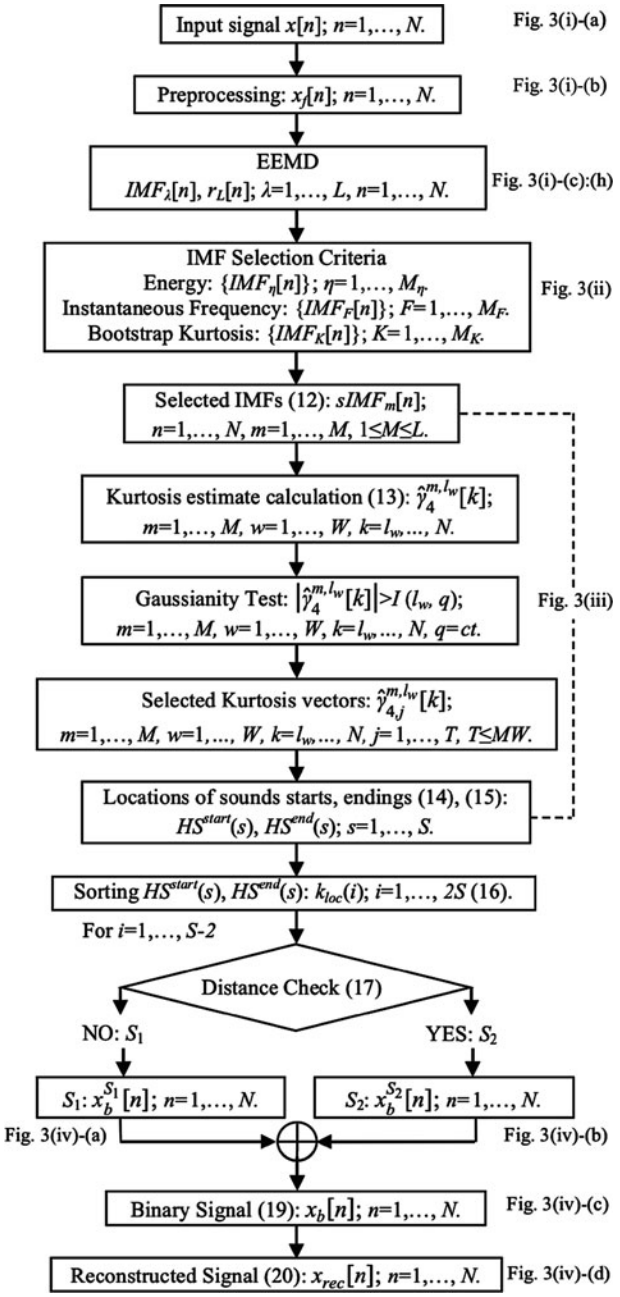

Fig. 2. Block diagram of the proposed HSS-EEMD/K scheme and the correspondence with the working example of Fig. 3.

where m is the number of the $sIMF$ ($m = 1, \ldots, M$), l_w is the wth sliding window ($w = 1, \ldots, W$), and k is the last sample of each sliding window, on which the calculated kurtosis estimate value is assigned to ($k = l_w, \ldots, N$). The window slides with one-sample shift until the last sample of the window coincides with the last sample of the heart sound segment. In this step, a total of $M \times W$ kurtosis estimate vectors are produced.

2) $\hat{\gamma}_4^{m,l_w}[k]$ *Selection:* Since the kurtosis estimate value depends on the window length within it is calculated, it is not certain that all $\hat{\gamma}_4^{m,l_w}[k]$ vectors will correspond to non-Gaussian kurtosis estimate values. Therefore, another Gaussianity test is performed at this point in order to use only the ones that comply with (5). Specifically, using the same q as in the IMF

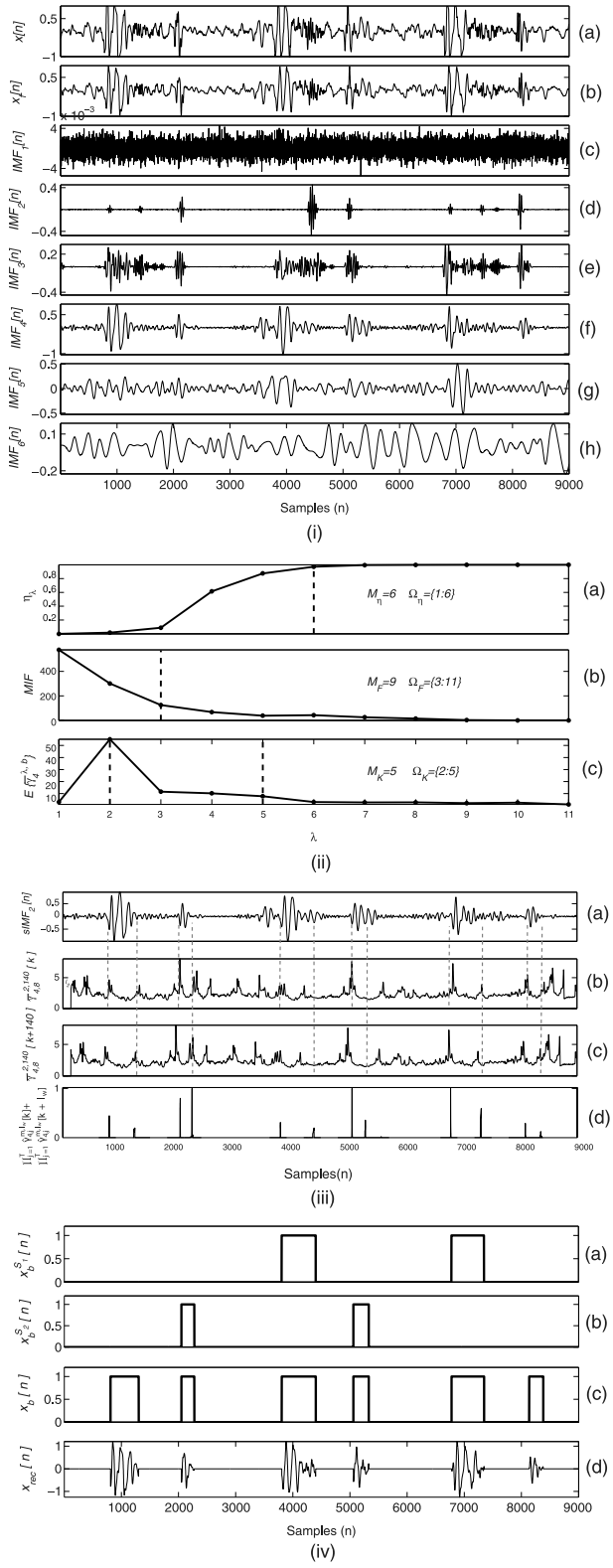

Fig. 3. Working example of the proposed method on a mitral regurgitation case. (i): (a) Original signal $x[n]$. (b) Preprocessed signal $x_f[n]$. (c)–(h) Six first IMFs. (ii): (a) Estimated η_λ. (b) *MIF*. (c) $E\{\hat{\gamma}_4^{\lambda,b}\}$ parameters and IMF selection according to (12). Here, $sIMF[n] = \{3{:}5\}$. (iii): (a) Second selected IMF ($IMF_4[n]$). (b) Example of the kurtosis estimate. (c) Shifted kurtosis estimate ($w = 2$, $l_w = 140$). (d) The normalized sum of the multiplied kurtosis and shifted kurtosis vectors for all m and l_w. (d) The dashed lines mark the sounds starts and ends finally proposed by the HSS-EEMD/K scheme. (iv): (a)–(c) Estimated binary signals of S_1, S_2, and ($S_1 + S_2$), respectively. (d) Corresponding reconstructed S_1 and S_2 signals of $x[n]$.

selection and (6), the confidence intervals $I(l_w, q)$ are calculated for each window. Then, each $\hat{\gamma}_4^{m,l_w}[k]$ vector is selected only if its maximum absolute value lies outside $I(l_w, q)$. Assuming that T $\hat{\gamma}_4^{m,l_w}[k]$ vectors are selected, they are denoted by $\hat{\gamma}_{4,j}^{m,l_w}[k]$, where $j = 1, \ldots, T$ and $T \leq M \times W$.

3) Heart Sound Starts and Ends Determination: Kurtosis ability to detect the changes along a signal is used to determine the starts and ends of the heart sounds. When a change occurs, e.g., when a sound starts or ends, the $\hat{\gamma}_{4,j}^{m,l_w}[k]$ value tends to become bigger. A more abrupt change results in a bigger kurtosis estimate value. To locate the sounds starts, all the $\hat{\gamma}_{4,j}^{m,l_w}[k]$ are multiplied. Since their value is bigger on the locations where a sound starts, the value of the product on the specific locations will be boosted. The hearts sound starts are thus defined as the locations where the derivative of the product obtains its maximum value. This is expressed as

$$\mathrm{HS}^{\mathrm{start}}(s) = \text{ Locations of max } \left[\mathrm{diff} \prod_{j=1}^{T} \hat{\gamma}_{4,j}^{m,l_w}[k] \right] \quad (14)$$

where $s = 1, \ldots, S$ and S is the number of the sounds starts found. One would expect that (14) would detect also the locations where the sounds end. However, the ends of the sounds, being close to the starts, appear shifted to the right. In particular, the shifting is proportional to the window length. To this end, each $\hat{\gamma}_{4,j}^{m,l_w}[k]$ undergoes a l_w left shift forming the $\hat{\gamma}_{4,j}^{m,l_w}[k + l_w]$ vectors. Then, the product of these $\hat{\gamma}_{4,j}^{m,l_w}[k + l_w]$ is calculated and the ends of the sounds are defined as the locations where its derivative obtains its maximum value:

$$\mathrm{HS}^{\mathrm{end}}(s) = \text{Locations of max } \left[\mathrm{diff} \prod_{j=1}^{T} \hat{\gamma}_{4,j}^{m,l_w}[k + l_w] \right]. \quad (15)$$

In (15), $\mathrm{HS}^{\mathrm{end}}(s)$ has to have the same length as $\mathrm{HS}^{\mathrm{start}}(s)$. Therefore, a check is performed to ensure that the heart sounds ends correspond to the heart sounds starts. According to the literature, a heart sound duration lies between 0.055 and 0.15 s [46]. For $s = 1, \ldots, S$, $\mathrm{HS}^{\mathrm{end}}(s)$ is expected to be found within the area $t = \mathrm{HS}^{\mathrm{start}}(s) + (0.055 \times F_s)$:$\mathrm{HS}^{\mathrm{start}}(s) + (0.15 \times F_s)$, where F_s denotes the sampling frequency; if otherwise, the maximum value of $\left[\mathrm{diff} \prod_{j=1}^{T} \hat{\gamma}_{4,j}^{m,l_w}[k + l_w]\right]$ within the area t is found and assigned to $\mathrm{HS}^{\mathrm{end}}(s)$. The chosen sound starts and ends locations, i.e., $\mathrm{HS}^{\mathrm{start}}(s)$, $\mathrm{HS}^{\mathrm{end}}(s)$, are then merged into one sorted vector, denoted by $k_{\mathrm{loc}}(i)$, $i = 1, \ldots, 2S$ according to the following equations:

$$k_{\mathrm{loc}}(i) = \begin{cases} \mathrm{HS}^{\mathrm{start}}(s), & \text{for } i = 1\colon 2\colon 2S-1 \quad (16a) \\ \mathrm{HS}^{\mathrm{end}}(s), & \text{for } i = 2\colon 2\colon 2S. \quad (16b) \end{cases}$$

Continuing the working example of Fig. 3, Fig. 3(iii)–(a) presents one of the selected IMFs ($sIMF_2[n]$), while Fig. 3(iii)–(b) and (c) correspond to the $\hat{\gamma}_{4,6}^{2,l_2}[k]$ and the shifted $\hat{\gamma}_{4,6}^{2,l_2}[k + l_2]$, respectively, both calculated on $sIMF_2[n]$. The locations of the starts and the ends of the sounds that the algorithm finally predicts using (14) and (15) are denoted with dashed lines. Fig. 3(iii)–(d) shows the normalized sum of $\prod_{j=1}^{T} \hat{\gamma}_{4,j}^{m,l_w}[k]$ and $\prod_{j=1}^{T} \hat{\gamma}_{4,j}^{m,l_w}[k + l_w]$, for $m = 1{:}3$, $l_w = 70{:}70{:}420$, and $T = 18$, as these values resulted by the algorithm. This signal is not later used in the algorithm, but is presented here to show how the peaks in the locations of the sounds are boosted after the multiplication of the $\hat{\gamma}_{4,j}^{m,l_w}[k]$ and $\hat{\gamma}_{4,j}^{m,l_w}[k + l_w]$ vectors, compared to peaks that may appear on some individual kurtosis vectors but do not correspond to sounds. This also explains why not all final peaks appear on every individual $\hat{\gamma}_{4,j}^{m,l_w}[k]$ or $\hat{\gamma}_{4,j}^{m,l_w}[k + l_w]$.

4) Discrimination between S_1 and S_2: The decision between S_1 and S_2 is based on the fact that in a cardiac cycle, the diastolic duration is longer than the systolic one. For $i = 1, \ldots, S - 2$, the following inequality is successively checked

$$k_{\mathrm{loc}}(2i+1) - k_{\mathrm{loc}}(2i) < k_{\mathrm{loc}}(2i+3) - k_{\mathrm{loc}}(2i+2). \quad (17)$$

If (17) is true, the area $k_{\mathrm{loc}}(2i + 1)$:$k_{\mathrm{loc}}(2i + 2)$ corresponds to an S_2, else it corresponds to S_1. The false results of (17), F case, form the binary S_1 vector while the true results of (17), T case, form the binary S_2 vector, as denoted by the following equations:

$$F\colon x_b^{S_1}[n] = \begin{cases} 1, & n \in [k_{\mathrm{loc}}(2i+1)\colon k_{\mathrm{loc}}(2i+2)] \quad (18a) \\ 0, & \text{elsewhere} \quad (18b) \end{cases}$$

$$T\colon x_b^{S_2}[n] = \begin{cases} 1, & n \in [k_{\mathrm{loc}}(2i+1)\colon k_{\mathrm{loc}}(2i+2)] \quad (19a) \\ 0, & \text{elsewhere} \quad (19b) \end{cases}$$

where $i = 1, \ldots, S - 2$. The case $i = 1$ performs a check for the definition of the second sound of the PCG signal. Similarly, for $i = S - 2$, the semifinal sound is determined. The first and the last heart sounds of the PCG signal are not included in the binary S_1, S_2 vectors. Hence, if for $i = 1$ the result of (17) is true, meaning that the second sound is an S_2, the first sound [$k_{\mathrm{loc}}(1)$:$k_{\mathrm{loc}}(2)$] is defined as an S_1 and vice versa. Correspondingly, the last sound [$k_{\mathrm{loc}}(2S - 1)$:$k_{\mathrm{loc}}(2S)$] is defined as an S_1, if for $i = S - 2$ (17) is true, or as an S_2, if it is false. The addition of the binary $x_b^{S_1}[n]$, $x_b^{S_1}[n]$ signals including the first and the last heart sounds provides the segmented binary PCG signal, defined as

$$x_b[n] = \begin{cases} 1, & n \in [k_{\mathrm{loc}}(2i+1)\colon k_{\mathrm{loc}}(2i+2)] \quad (20a) \\ 0, & \text{elsewhere} \quad (20b) \end{cases}$$

where $i = 0, \ldots, S - 1$. Finally, using (20), the original PCG signal can be filtered so that the first and second heart sounds are extracted by multiplying the binary $x_b[n]$ with the sum of the selected IMFs ($sIMF_m[n]$), as follows:

$$x_{rec}[n] = x_b[n] \sum_{m=1}^{M} sIMF_m[n] \quad (21)$$

where $n = 1, \ldots, N$. An example of the result of the application of the proposed scheme to the PCG signal of Fig. 3(i)–(a) is presented on Fig. 3(iv), where the binary signals $x_b^{S_1}[n]$ [see Fig. 3(iv)–(a)], $x_b^{S_2}[n]$ [see Fig. 3(iv)–(b)], $x_b[n]$ [see Fig. 3(iv)–(c)], and the reconstructed signal $x_{rec}[n]$ [see Fig. 3(iv)–(d)] are depicted.

TABLE I
CHARACTERISTICS OF THE EXPERIMENTAL TESTING DATASET

Category[a]	Subjects[b] No (Gender)-(Mean Age±std)-(Severity)	S_1-S_2 Cycle No
Controls	11 (4M/7F)-(29.3±10.7)	698
AS	16 (6M/10F)-(75.3±10.2)-(7MD/9SV)	827
MR	16 (6M/10F)-(76.1±7.2)-(10MD/6SV)	1077
Total	43 (16M/27F)-(63.7±22.4)	2602

[a]AS: Aortic Stenosis. MR: Mitral Regurgitation.
[b]M: Male. F: Female. MD: Medium. SV: Severe. Age is in years.

IV. IMPLEMENTATION ISSUES

A. Experimental Dataset

The PCG data used for the algorithmic development and testing of the HSS-EEMD/K scheme were recorded in the 1st Cardiac Clinic of Papanikolaou General Hospital in Thessaloniki, Greece. The database collected is composed of 52 different subject's records; in particular, 14 records come from controls, 19 records come from patients with aortic stenosis, and 19 records come from patients with mitral regurgitation. The diagnosis and the severity of the heart valve diseases were determined by the doctors, based on the echocardiogram of the patient, according to the recommended standards [47]. The samples were recorded from the auscultation position of the chest where the murmur is best heard for each valve dysfunction, while the normal heart sound samples were recorded from the apex. Recordings from more than one position could be used; however, they were avoided here, so to simulate a real auscultation examination with an electronic stethoscope and reduce the complexity of the implementation of the HSS-EEMD/K scheme, thus ensuring the applicability of the developed scheme in common clinical practice. From the total dataset, nine records, three of each category were used for the methodology's development; thus, the dataset that the HSS-EEMD/K method was tested on contains 43 heart sound records, 11 records from controls, 16 from patients with aortic stenosis, and 16 from patients with mitral regurgitation, forming a total of 2602 heart cycles (698 cycles of normal heart sounds, 827 aortic stenosis cycles, and 1077 mitral regurgitation cycles). The testing dataset consists of about 60% samples from women and 40% samples from men, within an age range of 16–90 years, and cases of medium and severe heart valve diseases. The characteristics of the testing dataset are summarized in Table I. The recordings of the heart sounds were performed using the electronic stethoscope AUDIOSCOPE, which records the signal amplified and unfiltered, and the software Audacity, with a sampling frequency of 44100 Hz, and a 16-bit resolution. Since normal and abnormal heart sounds have a frequency range of 50–700 Hz, the original PCG recordings were down-sampled from 44.1 to 4 kHz, zero-meaned, and normalized to [-1 1]; all sounds were stored in .wav format. The analysis was carried out on a personal computer using MATLAB R2011b (The Mathworks, Inc., Natick, MA, USA).

B. General Evaluation Indices

In order to produce a gold standard of the heart sounds, a manual evaluation process, performed by an independent expert physician, took place. The recorded PCGs were audio-visually reviewed, and the positions of the heart sounds peaks were marked via mouse-clicking. Adopting the following symbolisms, S_O for the observed sounds, i.e., the number of the sounds of the recorded PCG that the physician indicated, S_P for the predicted sounds, i.e., the number of sounds resulted by the application of the segmentation algorithm, and S_C for the correctly predicted sounds, i.e., the predicted sounds matching the observed sounds, the prediction power Q_P of the proposed method was measured as the geometric means of the ratios S_C/S_O and S_C/S_P

$$Q_P = 100\sqrt{\frac{S_C}{S_O}\frac{S_C}{S_P}}. \tag{22}$$

Q_P is an overall index that takes into account not only the detectability efficiency of an algorithm, but also its performance related to the false positives, i.e., the locations predicted by the algorithm that are not consistent with existing sounds. For each heart sound sample, a physician was asked to mark the peaks of the existing sounds. Then, for $i = 0, \ldots, S_O - 1$, the $i+1$ heart sound was assumed to have been correctly predicted when the area predicted by the algorithm $[k_{\mathrm{loc}}(2i+1){:}k_{\mathrm{loc}}(2i+2)]$, for $i = 0, \ldots, S_O - 1$ enclosed the $i+1$ marked peak. Moreover, the accuracy of the method, seen as the percentage of the correctly segmented cycles, was estimated as

$$C_P = 100\frac{N_C}{N_O} \tag{23}$$

where N_O is the number of the observed cycles and N_C is the number of the correctly segmented cycles. A cycle is considered to be correctly segmented when the S_1 and S_2 are included in the specific cycle, along with the S_2 preceding and the S_1 following the cycle are correctly predicted, while there are no false positives in the distances between them, ensuring that the durations of diastole and systole are also accurately delimited.

C. Parameter Selection

As far as the parameters used in the implementation of the HSS-EEMD/K are concerned, the energy contribution parameter η_λ was set equal to 0.99, meaning that the selected M_η IMFs contain 99% of the signal's energy. The Bootstrap method's number of repetitions b was set equal to 1000 to ensure a statistically large sample of $\hat{\gamma}_4^{\lambda,b}$ vectors. Probability q was initially set equal to 0.999. The higher q value, the stricter Gaussianity test is suggested. However, the estimation of both (10) and (6) depends on the length of the IMF; consequently, a predefined single q value may not be suitable for any length N. For the case that $M_K = 0$, meaning that no $E\{\hat{\gamma}_4^{\lambda,b}\}$ lies outside $I(N,q)$, q is iteratively reduced and the test is repeated until at least one IMF is included in the Ω_K set. Moreover, the kurtosis estimate was calculated using different sliding windows, with lengths of, $l_w = F_s/50{:}F_s/50{:}F_s/10$ samples, for capturing the fast and slow changes of the waveform.

TABLE II
MEAN PREDICTION POWER $\overline{Q_P}$ OF THE HSS-EEMD/K SCHEME ALONG WITH OTHER FOUR ALGORITHMS [17], [25], [15], [3]

	$\overline{Q_P}\pm$std (%)			
	Normal	AS	MR	Total
Subjects	11	16	16	43
Heart Sounds	1396	1654	2154	5216
HSS-EEMD/K	**99.33±1.23**	**89.68±7.37**	**94.68±4.18**	**94.56±6.58**
HSS-FEM	95.39±3.05	85.66±5.76	89.91±3.37	89.48±5.57
HSS-ETS	98.58±1.01	84.72±3.44	89.38±3.18	90±6.17
HSS-ET	96.37±4.7	83.9±7.63	84.91±7.91	87.49±8.73
HSS-DWT	93.94±5.1	83.79±5.91	80.03±5.47	84.98±7.76

TABLE III
MEAN ACCURACY $\overline{C_P}$ OF THE HSS-EEMD/K SCHEME ALONG WITH OTHER FOUR ALGORITHMS [17], [25], [15], [3]

	$\overline{C_P}\pm$std (%)			
	Normal	AS	MR	Total
Subjects	11	16	16	43
S_1-S_2 Cycles	698	827	1077	2608
HSS-EEMD/K	**97.98±3.52**	**72.83±12.43**	**78.35±9.21**	**83.05±15.14**
HSS-FEM	87.75±9.91	56.26±14.72	66.67±11.57	67.34±16.8
HSS-ETS	95.13±3.56	68.32±9.85	68.62±9.04	75.23±14.33
HSS-ET	92.55±9.03	65.66±18.74	66.11±20.28	72.7±20.77
HSS-DWT	84.24±12.86	54.56±16.47	57.57±11.48	63.27±18.42

V. RESULTS AND DISCUSSION

A. Experimental and Evaluation Results

Excerpts from the experimental results derived from the application of the HSS-EEMD/K scheme on the dataset are depicted in Fig. 4. In all cases, the positions of the peaks, as identified by the physician, are marked by an asterisk, and the locations of the sounds limits predicted by the algorithm are marked by dashed lines to facilitate the visual evaluation of the results. For the cases of Fig. 4(i)–(iv), (a) corresponds to recorded heart signals, while (b) corresponds to the segmented reconstructed signal $x_{rec}[n]$. From the comparison of $x_{rec}[n]$ with $x[n]$, it is clear that the HSS-EEMD/K successfully predicts the locations of S_1, S_2 and extracts the sounds, both in normal cases [see Fig. 4(i)] and in cases where severe murmurs are present and overlapping with the sounds [see Fig. 4(ii) and (iii)]. Moreover, Fig. 4(iv) shows the efficiency of the HSS-EEMD/K to pick up the heart sounds in a mild case of mitral regurgitation, where S_2 is faded and can hardly be visually identified.

The prediction power and the accuracy of the HSS-EEMD/K when applied to the experimental dataset are determined using (22) and (23). Due to the extensive size of the dataset, the mean values of indices Q_P and C_P, averaged on each data category and denoted by $\overline{Q_P}$ and $\overline{C_P}$, respectively, are adopted and shown in Tables II and III in bold. From these tables, it is clear that the HSS-EEMD/K scheme performs efficiently for the case of the normal heart sounds, as it correctly predicts almost all the observed sounds ($\overline{Q_P} = 99.33\%$) and correctly segments almost all 698 heart cycles ($\overline{C_P} = 97.98\%$). Results for the cases of aortic stenosis ($\overline{Q_P} = 89.68\%$, $\overline{C_P} = 72.83\%$) and mitral regurgitation ($\overline{Q_P} = 94.68\%$, $\overline{C_P} = 78.35\%$) are quite significant; it is, however, obvious that the presence of the

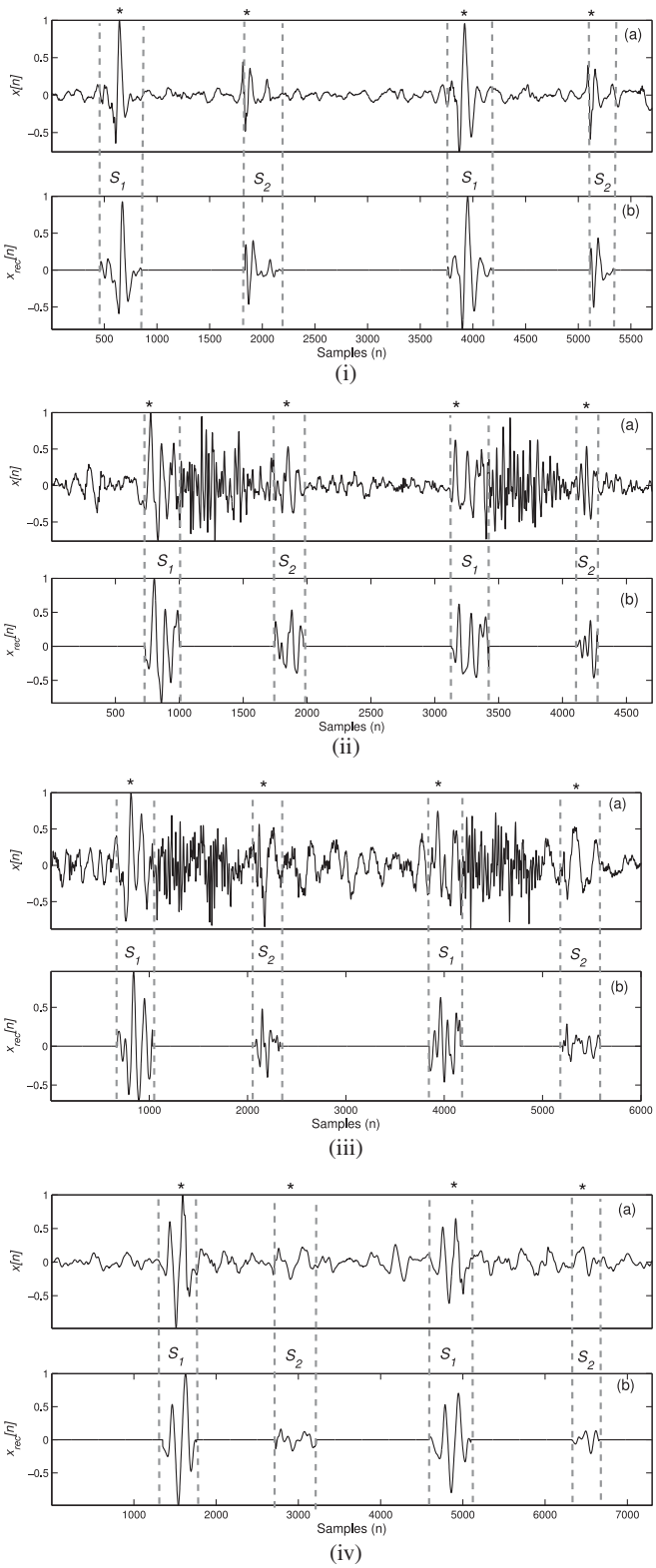

Fig. 4. Experimental results from the application of the HSS-EEMD/K scheme to real data. (i) Section of 5700 samples of a normal heart sounds case. (ii) Section of 4700 samples of a severe aortic stenosis case. (iii) Section of 6000 samples of a severe mitral regurgitation case. (iv) Section of 7300 samples of a medium mitral regurgitation case. In all cases (i)–(iv), (a) corresponds to the normalized initial PCG signal and (b) corresponds to the normalized reconstructed output of the HSS-EEMD/K scheme. The asterisks in all input data indicate the sounds peaks marked by the physician and the dashed lines indicate the sounds starts and ends proposed by the HSS-EEMD/K scheme.

murmurs leads to worse sound detection performance, compared to the normal case. The lower $\overline{Q_P}$ and $\overline{C_P}$ indices of aortic stenosis are mainly due to the high intensity of the murmurs present in some samples and to the S_2 fading in some cases of aortic stenosis, which makes the second heart sound hard to be detected. According to a study in [48], 73% of a group of patients with aortic stenosis were regarded as having a soft or single S_2, while in 9% of the patients, S_2 was absent. In the dataset used here, there are PCGs with an S_2 of very low intensity, as well as parts of murmurs that concur with the ends of the S_1 sounds. The latter is a problem commonly reported in segmentation approaches, e.g., in [49], a study on fetal phonocardiography, where the concurrence of parts of S_1 and S_2 with murmurs hampers their separation. Overall, the HSS-EEMD/K achieves a prediction power of 94.56% and an accuracy of 83.05% when applied to the experimental database. A detailed comparison with four other HSS methods is discussed in Section V-C.

B. Noise Stress Test

1) Additive Gaussian Noise: In order to examine the robustness of the proposed HSS-EEMD/K scheme, artificial noise testing, using different levels of noise contamination was performed. The recorded dataset consists of noisy heart sound signals and, thus, is inappropriate for the noise stress test, since the artificial noise would merge with the existing noise, resulting in an undefined signal-to-noise ratio. However, the performance of the HSS-EEMD/K method, as it was previously described, allows us to assume that the denoised, reconstructed signal $x_{rec}[n]$ serves as a close approximation of an original clean heart sound signal. Thus, $x_{rec}[n]$ is ideal to serve as the basis signal on which the noise test is performed. Note that the proposed method filters not only the noise present in a PCG, but also the murmur that it may contain in the cases of a heart valve disease. Nonetheless, the objective of the proposed method is to detect the locations of the first and the second heart sounds, classifying the presence of a murmur as a type of noise. Therefore, using heart sound signals devoid of murmurs does not eliminate any desirable information. To this end, a $x_{rec}[n]$ of three heart cycles (six heart sounds in total) was selected. Then, white Gaussian noise, localized to be adjusted to the desirable noise level at the occurrences of S_1 and S_2 was added to the selected $x_{rec}[n]$. The robustness of the method was tested for eight different levels of localized SNRs, denoted by LSNRs, specifically for noise contamination levels of $\{-15, -10, -5, 0, 5, 10, 20, 30$ dB$\}$. For each LSNR, white Gaussian noise was produced and added to the signal 50 times, leading to a set of 400 noisy signals $x_{noise}[n]$. It must also be noted that the denoised $x_{rec}[n]$ used was previously guaranteed the optimum values of the general evaluation indices, i.e., $Q_P = 100\%$ and $C_P = 100\%$. The general evaluation indices Q_P and C_P were calculated for the 400 noisy signals $x_{noise}[n]$ using (21) and (22), respectively, and their mean values for the eight different levels of LSNR, $\overline{Q_P}$ and $\overline{C_P}$, were obtained. Results of the noise stress test for the HSS-EEMD/K are graphically presented in error bars in Figs. 5–7(a). $\overline{Q_P}$ and $\overline{C_P}$ indices for different LSNRs for the HSS-EEMD/K scheme are shown in Figs. 5(i)–(a) and 5(ii)–(a). From these figures, the highly effective performance of the proposed method is apparent. More concretely, the $\overline{Q_P}$ index rapidly converges to 100% for LSNR values above 5 dB. For the high noise contamination LSNR of 0 dB, the proposed method still achieves a high mean prediction power of 87.72%. $\overline{C_P}$ index is also high for the different LSNRs, approaching 100% for LSNRs above 10 dB, and a value of 76% for the LSNR of 0 dB.

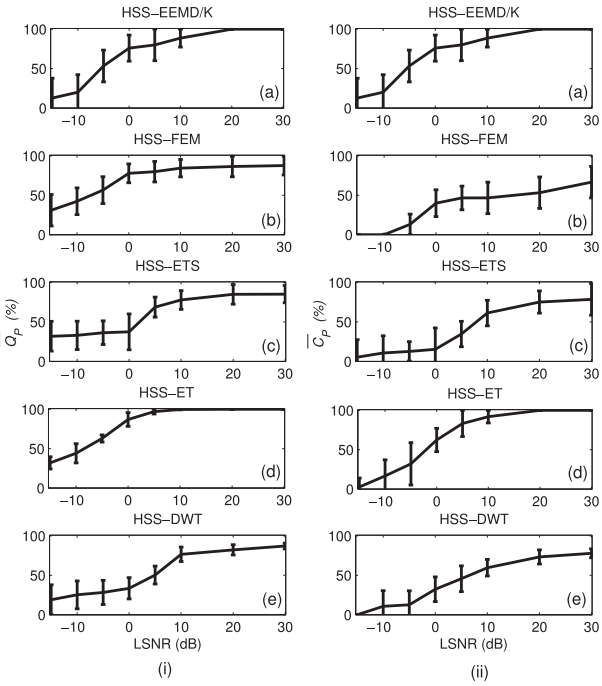

Fig. 5. Mean value (lines) and standard deviation (error bars) of noise stress test: (i) Q_P index and (ii) C_P index for different LSNRs. In both cases, (a), (b), (c), (d) and (e) correspond to the HSS-EEMD/K, HSS-FEM, HSS-ETS, HSS-ET, and HSS-DWT schemes, respectively.

The filtering that the proposed method performs also allows for the assessment of its ability to correctly predict the locations of the sounds starts and ends, as in the reconstructed signal, $x_{rec}[n]$, these specific locations are known. To this end, a scoring method was adopted, according to which the samples of the displacement of the predicted position from the observed position are counted. In the case of over-estimation, i.e., the predicted location lies outside the heart sound, the value of the displacement value is positive. Correspondingly, the negative value is used in the case of underestimation, i.e., the predicted location lies within the sound. The method scores zero when the predicted location coincides with the observed location. Index B was used to estimate the deviation from the true starts location, while index E represents the displacement from the observed ends. The total *termini* score TS for each sound is calculated as the sum of the absolute values of the B and E indices, as

$$TS = |B| + |E|. \tag{24}$$

Then, a TS value is characterized as TS_1, if the *termini* score was calculated from an S_1, or TS_2, if calculated from an S_2. This grouping is performed due to the fact that S_2 sounds tend to have shorter durations [46]; thus, lower values of mean TS

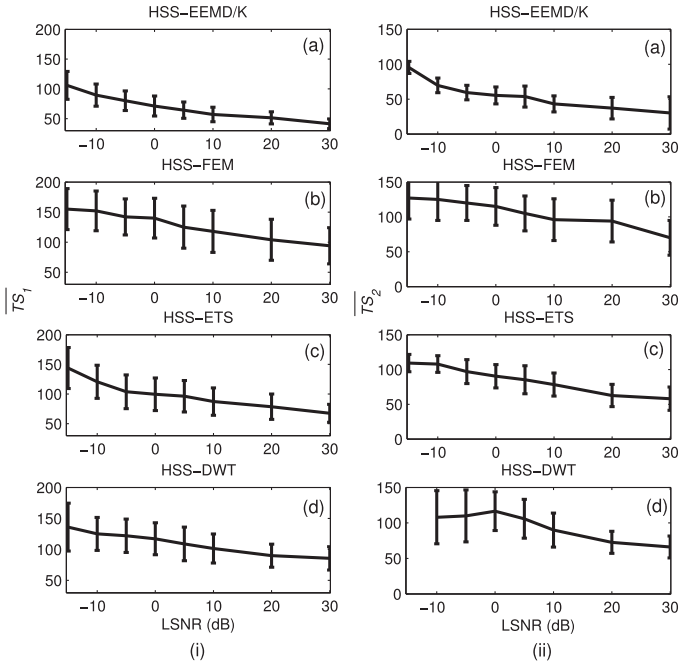

Fig. 6. Mean value (lines) and standard deviation (error bars) of noise stress test: (i) TS_1 index and (ii) TS_2 index for different LSNRs. In both cases, (a), (b), (c), and (d) correspond to the HSS-EEMD/K, HSS-FEM, HSS-ETS, and HSS-DWT schemes, respectively.

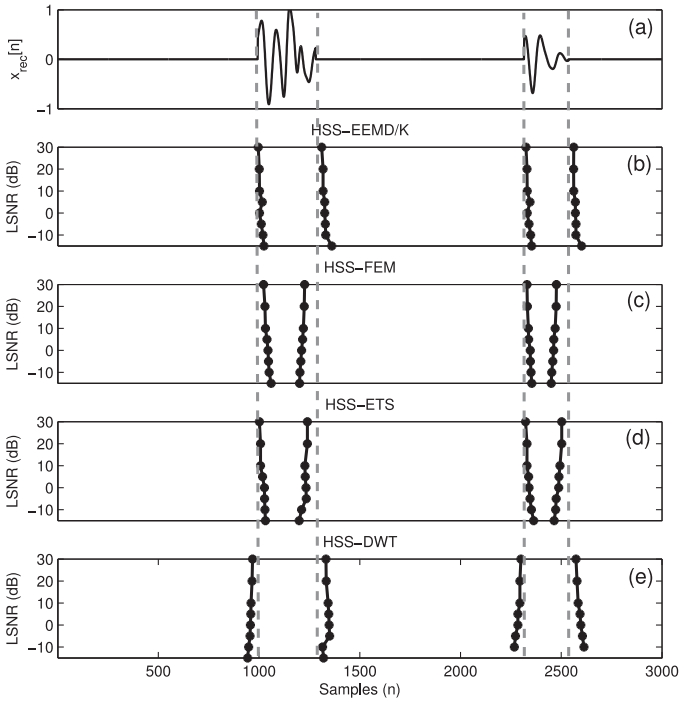

Fig. 7. Median value of the positions of the predicted starts and ends locations of two heart sounds for different LSNR levels: (a) two sounds from the $x_{rec}[n]$ used in the noise stress test, (b) the HSS-EEMD/K performance, (c) the HSS-FEM performance, (d) the HSS-ETS performance, and (e) the HSS-DWT performance. The dashed lines indicate the actual starts and ends positions.

are expected. The noise stress test evaluation indices B and E were averaged over the $x_{noise}[n]$ signals having the same LSNR and their mean values $\overline{TS_1}$ and $\overline{TS_2}$ were obtained. Fig. 6 depicts the *termini* scores $\overline{TS_1}$ [see Fig. 6(i)–(a)] and $\overline{TS_2}$ [see Fig. 6(i)–(b)] for the HSS-EEMD/K scheme. A lower TS index denotes a smaller deviation from the true locations of the sounds. At the noise level where the LSNR is equal to 30 dB, the proposed methods $\overline{TS_1}$ [see Fig. 6(i)-(a)] is 41.52 samples, while $\overline{TS_2}$ [see Fig. 6(ii)–(a)] is 30.23 samples. These values become meaningful by taking into account the sampling frequency of 4 kHz. Specifically, the mean B index for S_1 and for an LSNR of 30 dB is -11.29 samples, while the E index for the same conditions is 26.39, corresponding to a delay in the prediction of the heart sound start location of 2.8 ms (underestimation) and a delay in the prediction of the heart sound end location of 6.6 ms (overestimation). The same delays for the second heart sound at the LSNR of 30 dB are just 1.3 and 4.9 ms respectively. $\overline{TS_1}$ and $\overline{TS_2}$ gradually increase as the LSNRs decrease, to reach 105.98 and 95.57, respectively, for the LSNR of -15 dB.

Another parameter that can be deducted from the noise stress test implemented is the tendency of the HSS-EEMD/K scheme to underestimate or overestimate the heart sounds starts and ends. Fig. 7(a) shows two sounds from the $x_{rec}[n]$ used in the noise stress test, whereas Fig. 7(b) depicts the median value of the positions predicted in each LSNR by the HSS-EEMD/K. Results for the other two heart cycles of the $x_{rec}[n]$ were in accordance with those presented in Fig. 7(b). From the latter, it is clear that the proposed scheme exhibits a slight tendency to predict the starts of both sounds after the actual starts and the ends of the sounds after the actual ends. This tendency becomes more intense as the LSNR decreases, yet with values below zero. Moreover, it tends to predict the starts of the sounds closer to the actual starts, compared to the ends, i.e., B index is usually smaller in absolute value than E index for a particular combination of sound and LSNR. This is probably due to the fact that the start of a sound usually introduces a more abrupt change in the PCG signal.

2) Respiratory Noise: A second noise test was performed in order to test the robustness of the HSS-EEMD/K on a PCG contaminated with respiratory sounds. Following the example of [50], data of heart sounds ($HS[n]$), lung sounds ($LS[n]$), and their convolution were acquired,[1] forming the $s[n]$ signal, which was then used as an input to the HSS-EEMD/K scheme. Specifically, $s[n] = \sum_{q=1}^{2} \sum_{k=0}^{3} a_{qk} s_q[n-k]$, where $s_1[n] = HS[n]$, $s_2[n] = LS[n]$, a_q is the vector of FIR filter coefficients (a_1 was set equal to [0.8 0.9 1.1 1.2], while a_2 = [0.1 0.7 0.7 1.6]) and $n = 1, \ldots, 24000$. Sections of 6000 samples of the $HS[n]$, $LS[n]$, and $s[n]$ signals are shown in Fig. 8(a)–(c), respectively. The result of the segmentation and extraction of $s[n]$, i.e., $s_{rec}[n]$, is presented in Fig. 8(d). From the latter, the accurate detection, location, and reconstruction of the $HS[n]$ can be seen. The indices Q_P, C_P, $\overline{TS_1}$, and $\overline{TS_2}$ were calculated and the results are presented in Table IV in bold.

Related to the prediction power of the algorithm, HSS-EEMD/K was able to detect and extract 21 out of the 22 sounds

[1]Available at http://www.dundee.ac.uk/medther/Cardiology/hsmur.html and http://www.acoustics.org/press/132nd/2aea4.html.

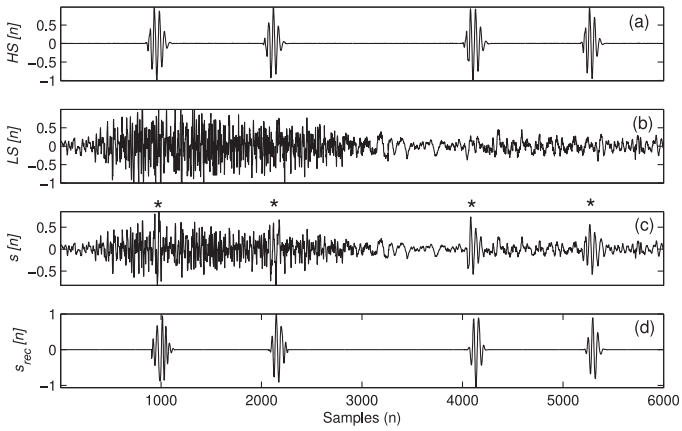

Fig. 8. Respiratory noise test signals and result: (a) 6000-sample segment of the normalized HS$[n]$, (b) 6000-sample segment of the normalized LS$[n]$, (c) normalized convolutive mixture of (a) and (b) $s[n]$, and (d) reconstructed by the HSS-EEMD/K $s_{rec}[n]$. Asterisks indicate the position of the HS$[n]$ in the $s[n]$ signal.

TABLE IV
RESPIRATORY NOISE TEST PERFORMANCE INDICES OF THE HSS-EEMD/K SCHEME ALONG WITH OTHER FOUR ALGORITHMS [17], [25], [15], [3]

	$Q_P(\%)$	$C_P(\%)$	$\overline{TS_1}$(n)	$\overline{TS_2}$(n)
HSS-EEMD/K	**97.7**	**91.67**	**50.55**	**45**
HSS-FEM	80.58	63.64	60.82	54.45
HSS-ETS	87.04	72.73	54.36	52.55
HSS-ET	84.24	72.72	-	-
HSS-DWT	79.77	54.55	58.36	54.91

correctly, while no false sound was proposed. This led to a correct segmentation of ten out of the 11 heart cycles. The sum of the deviations from the correct starts and ends location is low, as it can be deducted from the $\overline{TS_1}$ and $\overline{TS_2}$ values of Table III. Overall, the respiratory noise test revealed that the HSS-EEMD/K scheme performs efficiently even in the case of respiratory noise.

C. Comparison With Previous Works

The experimental and noise stress test results were compared to the indices values that stemmed from four efficient HSS methods when applied on the same experimental dataset. The techniques were chosen to include different methodologies, such as frequency- and energy-based analysis (HSS-FEM scheme [17]), complexity-based analysis (HSS-ETS scheme [25]), energy- and topology-based analysis (HSS-ET scheme [15]), and wavelet-based analysis (HSS-DWT scheme [3]). The HSS-FEM, HSS-ETS, and HSS-DWT schemes detect the duration of the heart sounds; hence, the same method as the one of the HSS-EEMD/K scheme was used to determine if one sound is predicted correctly, i.e., if the peak marked by the physician lies within the predicted location. However, the HSS-ET methodology detects one peak of each sound, yet not its duration. In order to determine whether one sound was predicted correctly in this case, the physician was asked to mark the starts and ends of the sounds. Then, a located sound was considered to be correctly predicted when its peak was detected between the marked start and end for the particular sound.

The corresponding results are tabulated in Tables II and III and depicted in Figs. 5(i),(ii)–(b):(e), 6(i),(ii)–(b),(d), and 7(c),(e). From the comparative results, it is evident that the implementation of the HSS-EEMD/K improved the evaluation indices $\overline{Q_P}$ and $\overline{C_P}$ in all three categories of samples and in total (see Tables II and III). The accuracy of 72% that the HSS-ET method achieved on the experimental database agrees with the one that it achieved on Vepa *et al.* 's database, according to [25]. Normal samples present satisfying results for all five methods; however, indices from the application of the algorithms on the valve diseases samples exhibit a decrement. It can be derived from Tables II and III that the decrease in both indices $\overline{Q_P}$ and $\overline{C_P}$ for both the categories of the aortic stenosis and mitral regurgitation samples is moderately bigger for the HSS-FEM, HSS-ETS, HSS-ET, and HSS-DWT schemes, when compared to the corresponding decreases of the HSS-EEMD/K scheme for most of the cases, showing that, overall, its performance appears to be less dependent on the presence of the murmurs.

For the noise stress test case, the Q_P and C_P indices could be calculated for all four schemes, yet the TS indices could only be calculated for the HSS-FEM, HSS-ETS, and the HSS-DWT schemes. This is owing to the fact that, as mentioned earlier, the HSS-ET scheme does not suggest a location for the start or the end of a heart sound but for its peak. Thus, the comparison was limited to the ability of the algorithms to detect the heart sounds and to segment the heart cycles. The comparison among the five methodologies, presented in Fig. 5, reveals that the HSS-EEMD/K and the HSS-ET schemes clearly exhibit more robust behavior than HSS-ETS, HSS-FEM, or HSS-DWT. HSS-EEMD/K achieves better $\overline{Q_P}$ and $\overline{C_P}$ indices for the majority of LSNRs; there are, however, LSNRs for which the HSS-ET's indices exceed the ones of HSS-EEMD/K. For example, for LSNR of 10 dB, $\overline{Q_P}$ of the HSS-ET is 99.67%, exceeding the 99.14% of the HSS-EEMD/K. In the case of the $\overline{C_P}$ index, the better performance of the HSS-EEMD/K scheme compared to the one of HSS-ET is clearer, since the curve of the HSS-ET degrades to a lower degree and with a faster rate, reaching the mean accuracy of 2.67% for and LSNR of -15 dB. The same accuracy for the HSS-EEMD/K is considerably higher, reaching 12.67%. As far as HSS-FEM, HSS-ETS, and HSS-DWT schemes are concerned, their indices have lower values at all LSNRs, indicating that they failed to correctly detect the sounds and to correctly segment the signals even in lower noise contamination conditions.

Moreover, both $\overline{TS_1}$ and $\overline{TS_2}$ of the proposed method have lower values for all LSNR levels compared to the ones achieved by the HSS-FEM, the HSS-ETS, or the HSS-DWT scheme (see Fig. 6). The displacement of the starts and ends true location increases for all other three methods as the LSNR decreases in both heart sounds. Note that in Fig. 6(ii)–(d), a value corresponding to the LSNR of -15 dB does not exist, due to the fact that HSS-DWT failed to detect any second heart sound during the noise stress test at the particular noise contamination level, thus a *termini* score could not be calculated. The low number of the correctly predicted second heart sounds is probably the cause for this curve decreasing after the LSNR of 0 dB, as the mean value calculated derived from few indicative samples. With reference

to the displacement tendencies of the HSS-FEM, the HSS-ETS, and the HSS-DWT methods, Fig. 7 shows that the HSS-FEM and HSS-ETS schemes tend to underestimate the duration of both heart sounds, while the HSS-DWT scheme tends to overestimate them. Once more, the HSS-DWT plot does not have a value corresponding to the LSNR of -15 dB for the reason previously mentioned.

Then, all methods were tested on heart sounds contaminated with a medium flow respiratory signal (see Section V-B.2). The results of the evaluation indices are presented in Table IV, from where it can be concluded that the proposed HSS-EEMD/K scheme detected more sounds compared to the other four approaches; thus, it correctly segmented more cycles, whereas the locations of the sounds starts and ends were averagely closer to the real ones, with the HSS-EEMD/K exhibiting the lowest $\overline{TS_1}, \overline{TS_2}$ values.

Finally, the contribution of the kurtosis criterion (see Section III) to the performance of the HSS-EEMD/K scheme was tested against the well-known statistical significance test (SST), proposed by Wu and Huang [51], applied on the same datasets. The experimental results have shown that the adoption of SST as a means to identify the IMFs with useful information resulted in a mean of 15–20% reduction of the total prediction power and accuracy, compared to the kurtosis-based ones, reported in Tables II and III. This is probably due to the existence of additional sound information sources (e.g., murmurs) at the IMF level, which, however, are not related to S_1 and S_2, and mislead the SST criterion to include redundant IMFs.

The authors believe that the improvement implemented by the proposed method is mainly owing to a more effective decomposition of the PCG into its' distinct components than the WT decomposition, as well as the lower dependence of the detection algorithm on amplitude values. Methods that use energy-based analysis are more prone to miss the low amplitude S_2, which often appears in aortic stenosis and mitral regurgitation PCGs, or to misinterpret the high energy murmurs as sounds. The HSS-FEM scheme uses both frequency and energy characteristics of the PCG; however, it requires dataset-based training, which causes this scheme's lower performance on the dataset used here and makes it less favorable for clinical application, where ability to perform well with new data is essential. In the HSS-EEMD/K scheme, apart from the parameters of Section IV-C, the rest were based on heart sounds characteristics-related literature or were automatically adjusted by the algorithm; thus, the method is expected to perform well in a wide range of datasets.

D. Sensitivity Analysis

A sensitivity analysis was performed for the parameters used in the proposed scheme to determine the influence of their variation on the experimental results. The analysis included the parameters not justified by the literature, i.e., energy threshold η_λ and confidence interval determining probability q and was implemented by repeatedly varying one parameter at a time while holding the other fixed, as selected in Section IV-C. Then, the change in the output was measured in terms of the $\overline{Q_P}$ index, averaged over the total dataset. Although q is automatically adjusted by the algorithm, constant values were assumed for the sensitivity analysis in order to examine its relation to the results, which are presented in Fig. 7. From the latter [see Fig. 9(a)], it can be deducted that the performance of the proposed method gradually declines as the energy threshold values scale down, owing mainly to the inability of the algorithm to select IMFs coinciding with the other two criteria's selected IMFs for low energy thresholds (below 0.3) in the case of certain data samples. The output appears to be less correlated with the variations of the q value [see Fig. 9(b)], indicating that a wide range of confidence intervals can lead to the selection of the IMFs that contain the HS characteristics.

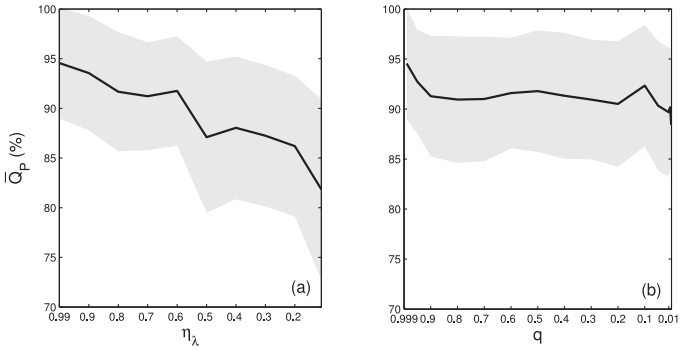

Fig. 9. Mean value (black line) and standard deviation (gray area) of $\overline{Q_P}$ index stemmed from the parameter sensitivity analysis for different values of (a) energy threshold η_λ and (b) confidence interval determining probability q.

E. Computational Cost

The computational cost of the HSS-EEMD/K scheme was defined by means of measuring the time needed to segment the heart sounds in a time interval of 1 s, i.e., in a PCG segment of 4000 samples. The time elapsed was 35.32 s, showing that the implementation needs improvement to be suitable for real-time analysis. EMD by definition follows an iterative process, whose computation time depends on the parameters set for the termination criteria. In EEMD, EMD is executed many times and an ensemble mean is taken from the IMF extracted, which highly increases the computational time. In the proposed method, 100 noise samples were used to extract the IMFs. However, efforts are being made to reduce the computational cost of the EMD. To this direction, the performance of the EMD is investigated in recent works, as in [52], where a statistical test for the exclusion of the IMFs with high-level noise components is implemented, thus, decreasing the processing time of the algorithm. Such techniques can be applied to the proposed method to increase its performance. The time needed for the proposed scheme to segment the cycle after EEMD is performed declines in 3.17 s, proving that EEMD is principally responsible for the long overall computational time. The times measured for the segmentation of the same PCG section are 0.36 s for the HSS-FEM scheme, 4 s for the HSS-ETS scheme, 0.14 s for the HSS-ET scheme, and 0.37 s for the HSS-DWT scheme, on an IBM-PC [Intel(R) Core(TM) i7 CPU/2.67 GHz].

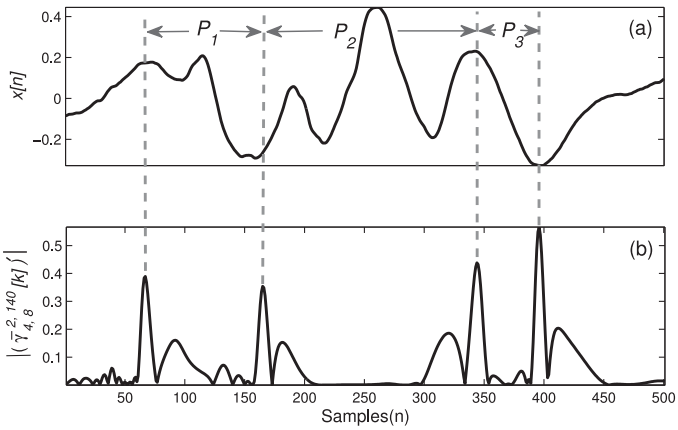

Fig. 10. Separation of a first heart sound into its three phases P_1, P_2, and P_3. (a) S_1 sound of the original PCG. (b) Absolute kurtosis first derivative, estimated on the second IMF along a sliding window of 140 samples. The dashed lines indicate the locations of the proposed phase separation, defined as the positions of the local maxima of the absolute kurtosis derivative.

F. Phase Separation

The duration of normal heart sounds was studied in [46]. According to this paper, the first and the second heart sounds consist of various vibrations having different frequencies. The extreme variability of the complexes of the heart sounds can make the separation of the components impossible in some cases. They developed, however, a simplified method to divide the sounds into three components, based on the idea that in both heart sounds, the main part of the sound includes larger vibrations, while the beginning and the end of the sound is formed by slower vibrations. As analyzed in Section II-C, kurtosis is able to detect the occurrences in a heart sound signal by detecting the deviations from Gaussianity. The kurtosis estimated along a sliding window presents peaks at the starts and the ends of the sounds, denoting the change of an event, as seen on the presentation of the proposed method (see Section III-C). It has been observed in many cases of sounds of the recorded database, especially in sounds belonging in the category of the normal samples, that the kurtosis vectors present peak values *within* a heart sound, implying some change of event within the sound. This becomes clearer when kurtosis is estimated using short-duration sliding windows, where shorter events also cause a sharp rise of the kurtosis value. An example is shown in Fig. 10, where the kurtosis is calculated on a selected IMF of a 500-sample S_1 signal from a normal case [see Fig. 10(a)], using a sliding window of 140 samples and its absolute first derivative is obtained [see Fig. 10(b)]. The signal contains one first heart sound. From Fig. 10, it can be seen that the local maxima of the absolute kurtosis derivative vector propose a separation of the sound into three phases P_1, P_2, and P_3, which is consistent with the separation made by Luisada *et al.* [46]. No methods of segmenting a heart sound into its components were found in the literature; nevertheless, indications of the kurtosis estimation show that it could be used toward this purpose for a deeper analysis of the heart sounds. The elaboration of this indicative result is left for a future work.

G. Overall Perspective

The results that have stemmed from the application of the HSS-EEMD/K scheme to the recorded dataset and from the noise stress test in overall surpass the ones of the HSS-FEM, HSS-ETS, HSS-ET, and HSS-DWT. However, they may not seem high enough in some cases. These are the cases of the mean prediction power $\overline{Q_P}$, and especially the mean accuracy $\overline{C_P}$ in the categories of aortic stenosis and mitral regurgitation. It has to be noted that the experimental dataset, recorded under hospital conditions, includes recordings of noisy ambience and samples of severe valve diseases, whose murmur can be very intense and overlapping with the first sound, hindering the detection of the sound and the prediction of its correct location. Moreover, there are cases where the second sound has completely faded, making the segmentation of the heart cycles impossible. Complete heart sound databases are available online; however, their main purpose being educational, they are deprived of any environmental noise and the cases of heart valve sounds chosen are such that the murmur can be distinguishable from the S_1 and S_2 sounds. Numerous previous works have used such databases to test their algorithms. Using this approach for the proposed method would most likely bring forth better sound detection and segmentation results; nevertheless, they would not correspond to the real results of the application of the method in actual clinical circumstances. Remarkably, a single, established database which would allow the objective comparison between the different HSS methodologies database has not yet been designed. However, this being the case, it is possible that many methods would adjust their parameters to achieve good results on the particular database. Moreover, as far as the C_P index is concerned, the criterion chosen for a heart cycle to be considered correctly segmented is considerably strict. Previous works do not mention their method followed to determine whether a heart cycle has been correctly segmented. Alternative approaches could be that a cycle is correctly segmented when its two sounds, the diastolic period prior to the first sound and the systolic period between the sounds, or the two sounds, the systolic period and the diastolic period after the second sound, are correctly predicted. The method adopted here, to denote a cycle correctly segmented when the two sounds, the diastolic periods before and after and the systolic in between, are correctly predicted, ensures that a segmented cycle will be correct from any point of the cycle, but decreases the value of C_P in the cases that there are falsely predicted sounds along the soundless parts of the cycles.

VI. Conclusion and Future Work

The HSS-EEMD-K scheme, a HSS and extraction method that employs ensemble EMD and kurtosis features proposed in this study, proved to be a promising tool for the detection and extraction of the first and second heart sounds, the determination of their durations, and the separation of the heart cycle into its four components (diastole-S_1-systole-S_2). The method was tested on an experimental database, recorded in real clinical environment, including normal heart sound samples, samples of aortic stenosis, and samples of mitral regurgitation. Given the difficulty posed by the recorded dataset, the experimental results show

reliable performance of the proposed method. Moreover, the extensive noise stress test implemented revealed its high robustness. The HSS-EEMD/K scheme can easily be implemented, and its computational cost can be reduced by improving the processing time of the EMD algorithm. Moreover, indications from the EEMD-based filtering and kurtosis estimation on a heart sound signal shed light upon a further segmentation; the separation of a sound into its structures. Comparison with other works validated the superior performance of the proposed scheme, in terms of detection power, accuracy, and noise robustness. Future work will focus upon the extension of the HSS-EEMD/K to the case of murmur identification and extraction from the raw PCG, facilitating the feature extraction process and the use of the segmented PCGs to build a valve disease identification tool.

ACKNOWLEDGMENT

The authors are grateful to the participants that contributed to form the large experimental dataset used here. They would also like to thank cardiologist N. Kipouridis for his help in acquiring the data, interpreting, and processing them.

REFERENCES

[1] R. T. H. Laennec and J. Forbes, *A Treatise on the Diseases of the Chest, and on Mediate Auscultation*. New York, NY, USA: Samuel S. and William Wood, 1838.

[2] B. Karnath and W. Thornton, "Auscultation of the heart," *Hospital Physician*, vol. 38, no. 9, pp. 39–43, 2002.

[3] J. Chebil and J. Al-Nabulsi, "Classification of heart sound signals using discrete wavelet analysis," *Int. J. Soft Comput.*, vol. 2, no. 1, pp. 37–41, 2007.

[4] D. Kumar, P. Carvalho, M. Antunes, J. Henriques, L. Eugenio, R. Schmidt, and J. Habetha, "Detection of S1 and S2 heart sounds by high frequency signatures," in *Proc. IEEE Conf. Proc. Eng. Med. Biol. Soc.*, 2006, vol. 1, pp. 1410–1416.

[5] D. Kumar, P. Carvalho, M. Antunes, J. Henriques, M. Maldonado, R. Schmidt, and J. Habetha, "Wavelet transform and simplicity based heart murmur segmentation," in *Proc. IEEE Comput. Cardiol.*, 2007, vol. 176, pp. 173–176.

[6] F. Meziani, S. M. Debbal, and A. Atbi, "Analysis of phonocardiogram signals using wavelet transform," *J. Med. Eng. Technol.*, vol. 36, no. 6, pp. 283–302, 2012.

[7] Z. Dokur and T. Olmez, "Heart sound classification using wavelet transform and incremental self-organizing map," *Digit. Signal Process. Rev. J.*, vol. 19, no. 3, pp. 951–959, 2008.

[8] H. Nazeran, "Wavelet-based segmentation and feature extraction of heart sounds for intelligent PDA-based phonocardiography," *Methods Inf. Med.*, vol. 46, no. 2, pp. 135–141, 2007.

[9] X. Zhang, L. Durand, L. Senhadji, H. C. Lee, and J.-L. Coatrieux, "Analysis-synthesis of the phonocardiogram based on the matching pursuit method," *IEEE Trans. Biomed. Eng.*, vol. 45, no. 8, pp. 962–971, Aug. 1998.

[10] W. Wang, Z. Guo, J. Yang, Y. Zhang, L.-G. Durand, and M. Loew, "Analysis of the first heart sound using the matching pursuit method," *Med. Biol. Eng. Comput.*, vol. 39, pp. 644–648, 2001.

[11] S. Jabbari and H. Ghassemian, "A time-frequency approach for discrimination of heart murmurs," *J. Signal Inf. Process.*, vol. 2, pp. 232–237, 2011.

[12] H.-H. Chen, T.-C. Chen, and L.-G. Chen, "Assessing normality of heart sound by matching pursuit residue with frequency-domain-based templates," in *Proc. IEEE Conf. Proc. Eng. Med. Biol. Soc.*, 2012, pp. 2917–2920.

[13] F. Hedayioglu, M. G. Jafari, S. S. Mattos, M. D. Plumbley, and M. T. Coimbra, "Denoising and segmentation of the second heart sound using matching pursuit," in *Proc. IEEE Conf. Proc. Eng. Med. Biol. Soc.*, 2012, pp. 3440–3443.

[14] H. Liang, S. Lukkarinen, and I. Hartimo, "Heart sound segmentation algorithm based on heart sound envelogram," in *Proc. IEEE Comput. Cardiol.*, 1997, pp. 105–108.

[15] S. Ari, P. Kumar, and G. Saha, "A robust heart sound segmentation algorithm for commonly occurring heart valve diseases," *Int. J. Med. Eng. Inform.*, vol. 32, no. 6, pp. 456–65, 2008.

[16] J. Martinez-Alajarin and R. Ruiz-Merino, "Efficient method for events detection in phonocardiographic signals," *Proc. SPIE*, vol. 5839, pp. 398–409, 2005.

[17] H. Naseri and M. R. Homaeinezhad, "Detection and boundary identification of phonocardiogram sounds using an expert frequency-energy based metric," *Ann. Biomed. Eng.*, vol. 41, no. 2, pp. 279–292, 2012.

[18] S. Choi and Z. Ziang, "Comparison of envelope extraction algorithms for cardiac sound signal segmentation," *Expert Syst. Appl.*, vol. 34, no. 2, pp. 1056–1069, 2008.

[19] L. Liu, H. Wang, Y. Wang, T. Tao, and X. Wu, "Feature analysis of heart sound based on the improved Hilbert-Huang transform," in *Proc. IEEE 3rd Int. Conf. Comput. Sci. Inf. Technol.*, 2010, vol. 6, pp. 378–381.

[20] Z. Zhao, Z. Zhao, and Y. Chen, "Time-frequency analysis of heart sound based on HHT [Hilbert-Huang transform]," in *Proc. Int. Conf. Commun., Circuits Syst.*, 2005, vol. 2, pp. 926–929.

[21] Z. L. Tseng, P. Y. Ko, and F. S. Jaw, "Detection of the third and fourth heart sounds using Hilbert-Huang transform," *BioMed. Eng. OnLine*, vol. 11, no. 8, pp. 1–13, 2012.

[22] A. Sepehri, A. G. T. Dutoit, A. Kocharian, and A. Kiani, "A novel method for pediatric heart sound segmentation without using the ECG," *Comput. Methods Progr. Biomed.*, vol. 99, pp. 43–48, 2010.

[23] Z. Yan, Z. Jiang, A. Miyamoto, and Y. Miei, "The moment segmentation analysis of heart sound pattern," *Comput. Methods Progr. Biomed.*, vol. 98, no. 2, pp. 140–150, 2010.

[24] V. Nigam and R. Priemer, "Accessing heart dynamics to estimate durations of heart sounds," *Physiol. Meas.*, vol. 26, pp. 1005–1018, 2005.

[25] J. Vepa, P. Tolay, and A. Jain, "Segmentation of heart sounds using simplicity features and timing information," in *Proc. IEEE Int. Conf. Acoust., Speech Signal Process.*, 2008, pp. 469–472.

[26] C. Gupta, R. Palaniappan, S. Swaminathan, and S. Krishnan, "Neural network classification of homomorphic segmented heart sounds," *Appl. Soft Comput.*, vol. 7, pp. 286–297, 2007.

[27] L. Gamero and R. Watrous, "Detection of the first and second heart sound using probabilistic models," in *Proc. IEEE 25th Annu. Int. Conf. Eng. Med. Biol. Soc.*, 2003, vol. 3, pp. 2277–2880.

[28] D. Gill, N. Gavrielli, and N. Intrator, "Detection and identification of heart sounds using homomorphic envelogram and self-organizing probabilistic model," *Comput. Cardiol.*, vol. 32, pp. 957–960, 2005.

[29] S. E. Schmidt, C. Holst-Hansen, C. Graff, E. Toft, and J. J. Struijk, "Segmentation of heart sound recordings by a duration-dependent hidden Markov model," *Physiol. Meas.*, vol. 31, no. 4, pp. 513–539, 2010.

[30] M. Fanfulla, M. Malcangi, M. Riva, D. D. Giustina, and F. Belloni, "Cardiac sounds segmentation algorithm for arrhythmias detection by fuzzy logic," *Int. J. Circuits, Syst. Signal Process.*, vol. 5, no. 2, pp. 192–200, 2011.

[31] H. Tang, T. Li, T. Qiu, and Y. Park, "Segmentation of heart sounds based on dynamic clustering," *Biomed. Signal Process. Control*, vol. 7, pp. 509–516, 2012.

[32] Z. Wu and N. Huang, "Ensemble empirical mode decomposition: A noise-assisted data analysis method," *Adv. Adapt. Data Anal.*, vol. 1, no. 1, pp. 1–41, 2009.

[33] N. Huang, Z. Shen, S. Long, M. Wu, H. Shih, Q. Zheng, N. Yen, C. Tung, and H. Liu, "The empirical mode decomposition and the Hilbert spectrum for nonlinear and non-stationary time series analysis," *Proc. Roy. Soc. Lond. A: Math. Phys. Eng. Sci.*, vol. 454, no. 1971, pp. 903–995, 1998.

[34] S. Charleston-Villalobos, A. Aljama-Corrales, and R. Gonzalez-Camarena, "Analysis of simulated heart sounds by intrinsic mode functions," in *Proc. IEEE Conf. Proc. Eng. Med. Biol. Soc.*, 2006, vol. 1, pp. 2848–2851.

[35] D. Boutana, M. Benidir, and B. Barkat, "Denoising and characterization of heart sound signals using optimal intrinsic mode functions," in *Proc. 4th Int. Symp. Appl. Sci. Biomed. Commun. Technol.*, 2011, pp. 1–5.

[36] A. Moukadem, A. Dieterlen, and C. Brandt, "Phonocardiogram signal processing module for auto-diagnosis and telemedicine applications," in *eHealth and Remote Monitoring*. A. H. E. Hassani, Ed. Rijeka, Croatia: InTech, 2012, ch. 7, pp. 117–136.

[37] S. Ari and G. Saha, "Classification of heart sounds using empirical mode decomposition based features," *Int. J. Eng. Inform.*, vol. 1, no. 1, pp. 91–108, 2008.

[38] J. Botha, C. Scheffer, W. W. Lubbe, and A. F. Doubell, "Autonomous auscultation of the human heart employing a precordial electrophonocardiogram and ensemble empirical mode decomposition," *Australas. Phys. Eng. Sci. Med.*, vol. 33, no. 2, pp. 171–183, 2010.
[39] I. Rekanos and L. Hadjileontiadis, "An iterative kurtosis-based technique for the detection of nonstationary bioacoustic signals," *Signal Process.*, vol. 86, no. 12, pp. 3787–3795, 2006.
[40] C. Saragiotis, L. Hadjileontiadis, I. Rekanos, and S. Panas, "Automatic P phase picking using maximum kurtosis and κ-statistics criteria," *IEEE Geosci. Remote Sens. Lett.*, vol. 1, no. 3, pp. 147–151, Jul. 2004.
[41] C. Nikias and A. Petropoulou, *Higher-Order Spectra Analysis: A Nonlinear Signal Processing Framework*. Englewood Cliffs, NJ, USA: Prentice-Hall, 1993.
[42] A. Papoulis, *Probability, Random Variables and Stochastic Processes*, 3rd ed. New York, NY, USA: McGraw-Hill, 1991.
[43] M. Kendall, A. Stuart, J. Ord, and K. Ord, *Kendall's Advanced Theory of Statistics*, 6th ed. New York, NY, USA: Wiley, 1994.
[44] P. Arnott, G. Pfeiffer, and M. Tavel, "Spectral analysis of heart sounds: Relationships between some physical characteristics and frequency spectra of first and second heart sounds," *J. Biomed. Eng.*, vol. 15, pp. 167–184, 2002.
[45] B. Efron, "The bootstrap and modern statistics," *J. Amer. Statist. Assoc.*, vol. 95, no. 452, pp. 1293–1296, 2000.
[46] A. Luisada, F. Mendoza, and M. Alimurung, "The duration of normal heart sounds," *Br. Heart J.*, vol. 11, no. 1, pp. 41–47, 1949.
[47] M. Quinones, C. Otto, M. Stoddard, A. Waggoner, and W. Zoghbi, "Recommendations for quantification of Doppler echocardiography: A report from the Doppler quantification task force of the nomenclature and standards committee of the American society of echocardiography," *J. Amer. Soc. Echocardiogr.*, vol. 15, pp. 167–184, 2002.
[48] P. Das, C. Pocock, and J. Chambers, "The patient with a systolic murmur: Severe aortic stenosis may be missed during cardiovascular examination," *Quarterly J. Medicine*, vol. 93, no. 10, pp. 685–688, 2000.
[49] F. Kovács, N. Kersner, K. Kádár, and G. Hosszú, "Computer method for perinatal screening of cardiac murmur using fetal phonocardiography," *Comput. Biol. Med.*, vol. 39, no. 12, pp. 1130–1136, 2009.
[50] F. Ghaderi, H. Mohseni, and S. Sanei, "Localizing heart sounds in respiratory signals using singular spectrum analysis," *IEEE Trans. Biomed. Eng.*, vol. 58, no. 12, pp. 3360–3367, Dec. 2012.
[51] Z. Wu and N. E. Huang, "A study of the characteristics of white noise using the empirical mode decomposition method," *Proc. Roy. Soc. Lond. A 8*, vol. 460, no. 2046, pp. 1597–1611, 2004.
[52] A. Karagiannis and P. Constantinou, "Noise assisted data processing with empirical mode decomposition in biomedical signals," *IEEE Trans. Inf. Technol. Biomed.*, vol. 15, no. 1, pp. 11–18, Jan. 2011.

Chrysa D. Papadaniil (S'10) was born in Serres, Greece, in 1985. She received the Diploma degree in electrical engineering from the Aristotle University of Thessaloniki (AUTH), Thessaloniki, Greece, in 2010. She is currently working toward the Ph.D. degree at AUTH, affiliated with the Signal Processing and Biomedical Technology Unit of the Telecommunications Laboratory.

Her current research interests lie in the area of advanced signal processing techniques and biomedical engineering concerning pathologies of the cardiorespiratory system.

Ms. Papadaniil is a member of the Technical Chamber of Greece.

Leontios J. Hadjileontiadis (S'87–M'98–SM'11) was born in Kastoria, Greece, in 1966. He received the Diploma degree in electrical engineering, in 1989, and the Ph.D. degree in electrical and computer engineering, in 1997, both from the Aristotle University of Thessaloniki (AUTH), Thessaloniki, Greece. He also received the Diploma degree in musicology from AUTH, in 2011, and the Ph.D. degree in music composition from the University of York, York, U.K., in 2004.

Since December 1999, he has been with the Department of Electrical and Computer Engineering, AUTH, as a faculty member, where he is currently a Professor, working on lung sounds, heart sounds, bowel sounds, ECG data compression, seismic data analysis, and crack detection in the Signal Processing and Biomedical Technology Unit of the Telecommunications Laboratory. He is also a Professor in composition at the State Conservatory of Thessaloniki, Thessaloniki, Greece. His research interests include higher order statistics, alpha-stable distributions, higher order zero crossings, wavelets, polyspectra, fractals, neuro-fuzzy modeling for medical, mobile, and digital signal processing applications.

Dr. Hadjileontiadis is a member of the Technical Chamber of Greece, the Higher-Order Statistics Society, the International Lung Sounds Association, and the American College of Chest Physicians. He received the second award at the Best Paper Competition of the ninth Panhellenic Medical Conference on Thorax Diseases97, Thessaloniki. He was also an open finalist at the Student paper Competition (Whitaker Foundation) of the IEEE EMBS97, Chicago, IL, USA, a finalist at the Student Paper Competition (in memory of Dick Poortvliet) of the MEDICON98, Lemesos, Cyprus, and the recipient of the Young Scientist Award of the twenty-fourth International Lung Sounds Conference99, Marburg, Germany. From 2004 till present, he has organized and served as a mentor to five student teams that excelled in the worldwide Imagine Cup Competition (Microsoft) [Sao Paulo, Brazil (2004)/Yokohama, Japan (2005)/Seoul, Korea (2007)/New York, NY, USA (2011)/Sydney, Australia (2012)] with projects involving technology-based solutions for people with disabilities. In this framework, he was awarded with the Champions Faculty Award 2012 in Sydney, Australia. Since 2012, he serves as an IEEE Student Branch Chancellor and in August 2013 he and his student team Symbiosis were awarded the IEEE Student Enterprise Award 2013.